ASIA TURBOMACHINERY & PUMP SYMPOSIUM
12 - 15 MARCH 2018
SUNTEC SINGAPORE

Using Digital Models for Condition Based Maintenance of High Pressure Pumps in SWRO Desalination Plants

Amr A. Abdel Fatah, Ph.D.
Mechanical Engineering Department
Centre of Excellence in Predictive Maintenance,
The British University in Egypt
El Sherouk City , Cairo, Egypt
amr.abdelkader@bue.edu.eg

Mohamed Lotfy, Ph.D.
Department of Mechanical Engineering,
Faculty of Engineering, Suez Canal University,
Ismailia, Egypt
Centre of Excellence in Predictive Maintenance,
The British University in Egypt,
El Sherouk City, Cairo, Egypt
mohamed.lotfy@bue.edu.eg

Mohammed A. Hassan, Ph.D.
Department of Electrical Engineering,
Fayoum University, Fayoum, Egypt.
Centre of Excellence in Predictive Maintenance,
The British University in Egypt
El Sherouk City , Cairo, Egypt.
hassanm@fayoum.edu.eg

Antoine S. Dimitri, Ph.D.
Mechanical Design and Production Department
Faculty of Engineering
Cairo University
Giza, Egypt
adimitri@eng.cu.edu.eg

Abstract

Condition based maintenance (CBM) is a very useful technique built around the concept of monitoring the operation of assets. This allows performing diagnostics, troubleshooting and determining the proper maintenance action. Conventional CBM programs are solely built around analyzing sensors' data collected from physical systems. Incorporating simulation data collected from digital replica of the system with sensors' data can lead to more optimization for operation and maintenance. This paper focuses on demonstrating the role of digital models in implementing effective condition based maintenance on high pressure pumps in SWRO desalination plants. Two digital models have been developed for the high pressure pump experiencing cavitation condition. The first digital model is a 3-D fully turbulent Computational Fluid Dynamic (CFD) model. Based on the pressure distribution obtained from the CFD model, pressure pulsation due to impeller-diffuser interaction is studied and used to analytically model the exciting forces affecting the rotor. The second digital model is a pump rotordynamic model which is used to predict the rotor vibration response to exciting forces at both normal and faulty operating conditions. Results obtained from the digital models are validated using an experimental test rig of a small centrifugal pump. Using this concept, a pump faulty operation can be simulated to provide complete understanding of the root cause of the fault. Additionally, digital models can be used to simulate different corrective actions that would restore the normal operation of the pump.

Introduction

Fresh water shortage is threatening development and prosperity in many Arab countries. In just ten years about two thirds of the Arab countries are expected to suffer from acute water scarcity. Sea Water Reverse Osmosis (SWRO) desalination is fast becoming a dominant technology for facing water shortage threats by cost effective production of fresh water for multiple purposes. The high pressure pump is the heart of any Reverse Osmosis desalination plant. The role of the high pressure pump is to raise the pressure of the feed flow to allow for the permeation process through the RO membranes. Typical pressures for SWRO are in the range of 40 – 80 bar. Accordingly, the high pressure pump consumes most of the electric energy supplied to the SWRO desalination plant.

Common problems experienced by a centrifugal high pressure pump may be attributed to one or several probable causes. Low flowrate or low pressure problem can be attributed to either air leaks in inlet piping or faulty mechanical seal. Pump cavitation can lead also to the same problem. Other common problems are excessive lateral or axial vibration and noise which can be attributed to either pump cavitation or to pump rotor misalignment or excessive axial thrust.

Cavitation can be considered as a major cause for pump failures. In the first phase of cavitation, vapor bubbles are formed in areas of relatively low pressure around the impeller of the pump. While in the second phase of the cavitation, the collapse of these bubbles triggers intense shockwaves leading to high speed fluid

impact causing significant pitting and erosion of the pump internal parts.

Condition based maintenance is built around the concept of monitoring the operation of assets. This will allow performing diagnostics, troubleshooting and determining the proper maintenance action. Digital models for a high pressure pump can be used to simulate different operating conditions and explain the resulting pump performance. A pump faulty operation can be simulated, thus providing complete understanding of the root cause of the fault. Additionally, digital models can be used to simulate different corrective actions that would restore the normal operation of the pump.

This paper focuses on demonstrating the role of digital models in implementing effective condition based maintenance on high pressure pumps in SWRO desalination plants. Two digital models have been developed for the high pressure pump experiencing cavitation condition. The first digital model is a 3-D fully turbulent Computational Fluid Dynamic (CFD) model. The second digital model is a pump rotordynamic model.

The CFD digital model is adopted for the prediction of the hydraulic performance of the high pressure pump under different operating conditions by visualizing the flow field inside the pump. Using the pressure field calculated from this digital model, distinct phases of cavitation can be detected. At cavitation condition, the CFD model allows the hydraulic efficiency deterioration of the pump to be monitored and corrective maintenance actions to be simulated. A safe range of operation with variable flowrates and variable rotational speed can be determined.

The pump rotordynamic model is developed using finite element four degrees of freedom beam element. Each node has two translation and two rotation motions in the plane. The rotor rotating parts dynamic characteristics are modeled including the masses, mass moment of inertias, and the gyroscopic effect. Moreover, this digital model incorporates the bearings dynamic characteristics. Using the rotordynamic model, the rotor critical speeds are determined and calibrated with the actual system.

Different excitations experienced in actual high pressure pump operation such as rotor unbalance and misalignment are modeled and the resulting rotor vibration spectrum can be investigated. At different phases of cavitation, the dynamic response of the rotor is obtained by exciting the digital model using an analytic model for the pressure pulsations.

Performance of the above introduced digital models is validated using an experimental test rig of a small centrifugal pump. The test rig is equipped with data acquisition and transducers to measure and record the rotational speed, flowrate, and the pump's inlet and outlet mean static pressure. Accelerometers are installed on the casing and the rotor of the pump to collect vibration signals.

The test rig is operated at the same operating conditions of different flowrates to obtain different phases of cavitation. Spectral signatures of the vibration signals collected experimentally are found to be in an excellent agreement with the dynamic response of the digital model of rotor during cavitation. The vibration excited due to the cavitation fault corresponding to the blades passing frequency is clearly observed in the measurements and simultaneously predicted in the digital models. This allows diagnosing the cavitation fault.

Concept of Using Digital Models for Condition Based Maintenance

Once the digital models of the pump are built, the associated performance of the pump under different operating conditions can be simulated. Different simulation scenarios can be useful in the context of predictive maintenance. For example, if a high vibration level is detected at the pump's casing, flow and pressure measurements are fed to the CFD model whose results shows bubbles formation and pressure fluctuation acting on both the pump's casing and rotor. The resulting force can be modeled and used to excite the rotordynamic model. The response of the digital models can then be compared to the actual vibration spectrum of the physical system to confirm the existence of cavitation. Moreover, once the fault is confirmed, its recommended corrective action can be virtually tried on the digital models to restore the normal operating condition before even applying it to the actual physical system. This concept of using digital model in fault detection and correction is illustrated in Figure 1. Another interesting application of using digital models in predictive maintenance is simulating the performance of the pump under harsh and destructive operating conditions (which cannot be physically tested) to estimate the remaining useful life of the system.

CFD Model

Predicting the performance of centrifugal pump under different operating conditions can be of a great use when applied to the area of predictive maintenance. Using digital models with CFD approach, as a numerical simulation technique, is of a great importance to reduce cost due to trial and error experiments in addition to its basic role in shortening the design cycle. The flow in centrifugal pump is very complex because it is turbulent and three dimensional in nature. The results obtained from CFD simulation can give a reasonable indication for condition

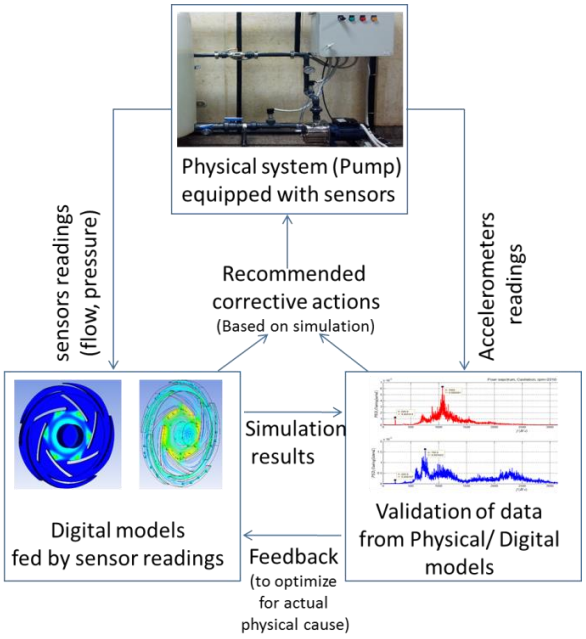

Figure 1. Concept of Using Digital Models for Fault Detection and Correction

evaluation and visualize the flow behavior inside the pump.

In the current study, a digital model is developed for the pump to study its behavior during different flow conditions. The effect of Shear Stress Transport (SST) turbulence model on the flow field for a single stage centrifugal pump with diffuser is investigated. A transient solution is obtained using ANSYS CFX software package.

The governing equation is a three-dimension incompressible Reynolds-Averaged Navier-Stokes equation for a single-phase analysis. Moreover, Equation (1) represents the Rayleigh-Plesset model. Both equations are used together on cavitation analysis (Kim et al. 2012). The vapor bubble growth and collapse on liquid is ruled by Rayleigh-Plesset equation.

$$R_b\ddot{R}_b + \frac{3}{2}\dot{R}_b^2 + \frac{2\sigma_s}{\rho_f R_b} = \frac{P_v - P}{\rho_f} \qquad (1)$$

In this equation, R_b, σ_s , ρ_f , P_v, and P refer to radius of bubble, surface tension coefficient, density of fluid, saturate vapor pressure, and pressure of fluid around vapor, respectively.

The centrifugal pump used in this study is a five-diffusers type closed impeller pump. Geometrical modelling of the pump components, Figure 2 , are done using SolidWorks. The dimensions of the impeller are as follows:

Impeller inlet diameter = 37 mm
Impeller outlet diameter = 130 mm
Blade thickness = 5 mm
Blade inlet width = 9.6 mm
Blade outlet width = 55.7 mm
β_inlet = 45 degree angle
β _outlet = 33.8 degree angle

The impeller is enclosed in a five vanned diffuser through which the water flow is discharged.

Meshing

Spatial discretization of the whole domain into finite volumes is done by ANSYS CFX. The mass, energy, and momentum quantities are stored in such volumes. In the current study, six bladed pump impeller with a containing diffuser are meshed with non-structured meshing in tetrahedral cells as shown in Figure 3. The whole mesh contains 44931 nodes and 204425 elements.

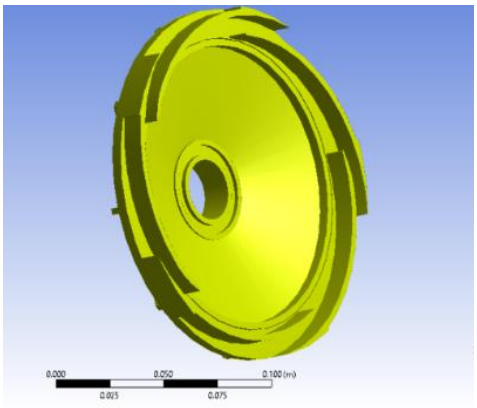

(a) Five-Vanned Diffuser

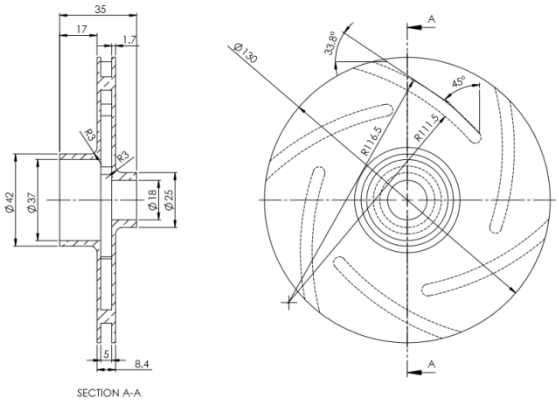

(b) Six-Bladed Impeller

Figure 2. The Geometric Model of the Impeller and Diffuser of the Centrifugal Pump

Boundary and Operating Conditions

The inlet boundary conditions are given as a volume flowrate at impeller eye and static pressure at diffuser outlets, Figure 4. The faces of the impeller flow zone are set as a rotating faces with no slip wall

condition. A stationary flow zone is applied to the diffuser. An isothermal model is adopted with incompressible water at 25° C. 3150 rpm constant angular speed is applied. For the cavitation, 15 Liter/min. inlet flowrate at impeller eye and 200,000 Pa static pressure at diffuser outlets are set to the digital model. For corrective action, 55 Liter/min. inlet flowrate at impeller eye and 300,000 Pa static pressure at diffuser outlets are set to the digital model. The residual convergence criterion is set as 1e-4.

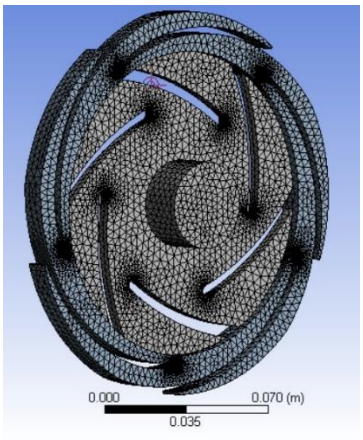

Figure 3. Flow Zones inside Impeller and Containing Diffuser

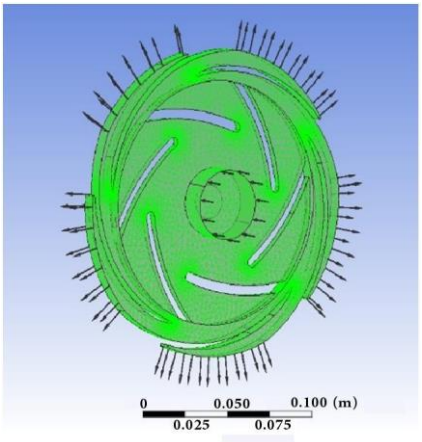

Figure 4. Impeller Inlet and Diffuser Outlets with Applied Boundary Conditions on the Digital Model

Pump Rotor Model

The development of a digital model for the pump's rotor enables understanding its behavior and the anticipation of its response to various sources of excitations. Faulty operation of the equipment will give rise to specific exciting forces.

The sources of the pump's vibration originate from different roots. Unbalance causes synchronous vibration (1X) corresponding to the frequency of rotation. While, the presence of coupling misalignment excites mainly the second harmonic (2X), in addition higher harmonics may also be excited (Piotrowski 1996)(Dewell and Mitchell 1984).

In centrifugal pumps, cavitation may occur when the inlet pressure becomes less than the vapor pressure causing high pressure pulsations (Xu, et al. 2017)(Shi, et al. 2017). Cavitation is detected by the remarkable increase of the vibration corresponding to the impeller blade passing frequency. The occurrence of such a fault results severe damage of the pump.

A condition based maintenance procedure can effectively be implemented by comparing the actual vibration spectrum of the equipment to the predicted results of a calibrated rotor digital model (Kallesøe, et al. 2006)(Sakthivel, et al. 2010). The analysis of the measured vibration enables defining the root cause of the vibration and thus fixing it.

In this work, a dynamic model for the pump's rotor is developed. The rotor response to unbalance and cavitation is simulated showing the dominant frequency excited in each case. In addition, an analytical model is proposed for modeling the pressure pulsations associated with cavitation.

Rotor Mathematical Model

The rotor is modeled by means of its mass 'M', gyroscopic 'G', and stiffness 'K' matrices, and the external forces 'F' applied to the rotor such as the unbalance, and cavitation excited forces. The rotor bearing equation is derived as,

$$M\ddot{X} + (C + \Omega G)\dot{X} + KX = F \tag{2}$$

The system equation is represented in the state space form for the system dynamic simulation,

$$\begin{Bmatrix} \dot{X} \\ \ddot{X} \end{Bmatrix} = \begin{bmatrix} 0 & I \\ -M^{-1}K & -M^{-1}(C+\Omega G) \end{bmatrix} \begin{Bmatrix} X \\ \dot{X} \end{Bmatrix} + \begin{Bmatrix} 0 \\ M^{-1}F \end{Bmatrix} \tag{3}$$

The rotordynamics are modeled by the augmented state space matrix where the system mass, stiffness, and damping characteristics are included. The system state vector 'X' represent the rotor degrees of freedom, which are the displacements in the horizontal and vertical directions as well as the rotor inclination angles in the horizontal and vertical planes. While the states '$\dot{X}$' are the states derivatives with time representing the linear and rotational velocities of the rotor nodes. The force vector 'F' represent the vector of external forces acting on the rotor.

Pump Rotor Model

In order to simulate the rotor system using the state space formulation presented by Equation (3), the augmented state space matrix which represents the dynamics of the system must be formulated including the mass, stiffness, and damping characteristics of the

rotor parts. The rotor consists of the shaft elements, discs, and bearings. The pump rotor system is modeled using the finite elements method.

The shaft is divided into a number of beam elements having continuous mass and elastic characteristics. Each beam element consists of two nodes with four degrees of freedom each: two translational and the other two are rotational. The beam element is expressed using the Euler Bernoulli beam element formulation. These beam elements are assembled in the assembly matrices 'M' and 'K' representing the mass and stiffness characteristics of the shaft.

On the other hand, the pump impeller, motor rotor and fan are modeled using disc element where the translational mass, the polar moment of inertia, and transverse moment of inertia are considered. The disc element is assumed to be rigid with modeled gyroscopic effect modeled by the matrix 'G'. Each disc element is attached to the shaft at the node that corresponds to the disc location. The bearing supports are added to the rotor model through the bearings characteristics described by their stiffness and damping coefficients.

The described rotor finite element 'FE' model is implemented on the pump rotor studied case. The rotor FE model is shown in Table 1.and illustrated in Figure 5. The shaft diameter is 15 mm and its length is 251 mm. The rotor material is steel of 7800 kg/m^3 density and 210 GN/m^2 modulus of elasticity.

The free vibration analysis is carried on to compute the rotor critical speeds and compare with the identified one in order to calibrate the system model. The critical speeds are computed by calculating the eigen values of the system augmented state space matrix. The experimentally identified rotor first critical speed is found to be 196 Hz corresponding to bearing stiffness of 3.6x10^6 N/m as illustrated in Figure 6.The rotor critical speeds are 196 Hz and 241 Hz.

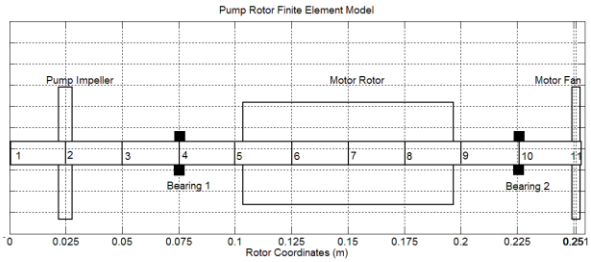

Figure 5. Rotor Finite Element Model

Experimental Setup

Experimental investigation is conducted using a closed circuit hydraulic test rig shown in Figure 7. This test rig allows for studying the centrifugal pump's performance and characteristics during different states of healthy and faulty conditions. The test rig is equipped with data acquisition and transducers to measure and record the impeller rotating speed, flowrate, the pump's suction and discharge pressures.

Table 1. Rotor Finite Element

Key Point	Axial Position (mm)	Disc Mass (kg)/ Transverse Moment of inertia (kgm^2)/ Polar Moment of Inertia (kgm^2)	Bearings Location
1	0.0		
2	25.1	Pump Impeller 0.5073 /5.29 x 10^{-4} / 1.03 x10^{-3}	
3	50.2		
4	75.3		B1
5	100.4		
6	125.5		
7	150.6	Motor Rotor 2.264 / 5.05x10^{-4} / 1.01 x10^{-3}	
8	175.7		
9	200.8		
10	225.9		B2
11	251	Motor Fan 0.04 / 1.59 x10^{-5} / 3.18 x10^{-5}	

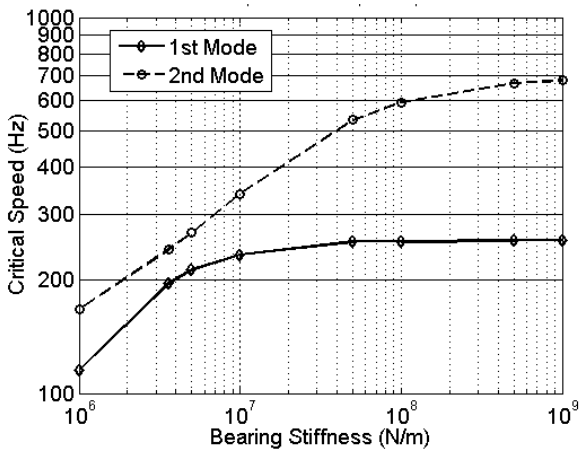

Figure 6. Pump Rotor Critical Speed Map

Two pressure transmitters with measuring ranges of zero to six bar and of zero to 10 bar are installed at the suction and the discharge of the pump, respectively. A flow meter with a measuring range of zero to 100 Liter /min is installed at the outlet of the pump. Two accelerometers are installed at the radial and axial positions on the casing of the pump to obtain vibration signals during different operating conditions of the pump, and two other accelerometers are installed at the driving end (DE) and non-driving end (NDE) of the electrical motor driving the pump. The accelerometers

are piezoelectric vibration acceleration sensors with frequency range of 0.5 to 10,000 Hz. The inlet pressure and the outlet flow are controlled by flow control valves.

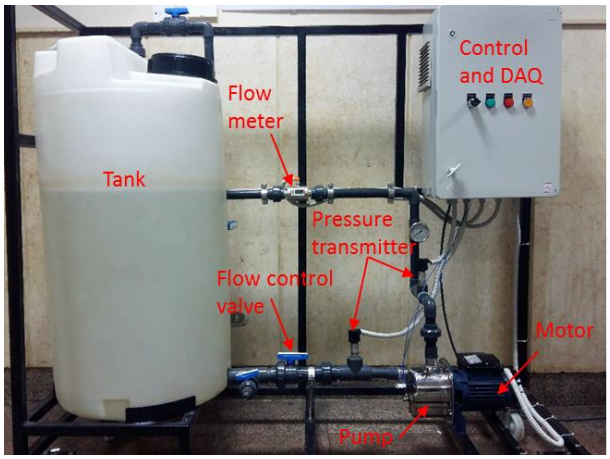

(a) Experimental Test Rig

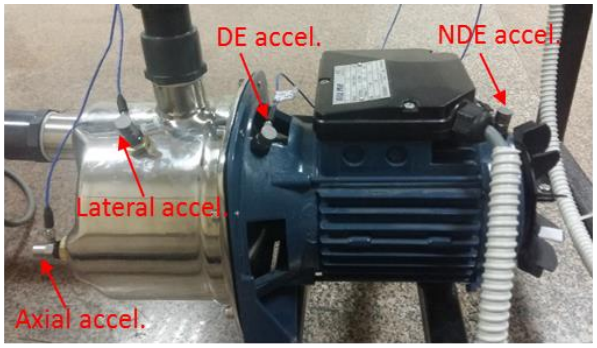

(b) Accelerometers Locations on the Pump
Figure 7. Experimental Setup

Vibration Monitoring of Centrifugal Pumps

Vibration characteristics have been widely used as effective methods for condition monitoring and health assessment of rotating machinery, including centrifugal pumps (Lu, et al. 2017). Pump vibrations reveal important information indicative to its running condition, incipient faults and component failure. By measuring and analyzing the vibration of a pump, nature and severity of the defect can be determined, and hence remaining useful life or expected failure point can be predicted. External vibrations measure on a pump is used to monitor the operating condition of the pump and diagnose the fault without interfering with the normal operation. Vibration analysis has been used in the literature to detect and characterize different types of pump problems ranging from hydraulic failures (such as cavitation, pressure pulsations, radial thrust, and axial thrust) (Xu, et al. 2017)(Shi, et al. 2017)(McKee, et al. 2011) to mechanical failures (such as bearing failure, seal failure, and impeller failure) (Abdulkarem, et al. 2014)(Golbabei, et al. 2009)(Abdel-Rahman and El-Shaikh 2009).

Spectral analysis of vibration signals is the most common and popular technique used in the field of condition monitoring of rotating machinery (Hassan, et al. 2014a). Measured vibration signals often carry dynamic information from mechanical elements. Spectral contents of these signals normally consist of fundamental frequencies of rotating components and their harmonics. When a mechanical element is damaged or worn, the energy of vibration increases at specific frequencies related to the revolutions of the defected rotating component (Farkokhzad, et al. 2014). Power spectrum is one of the most commonly used signal processing techniques for fault diagnosis in frequency domain (Hassan, et al. 2014b). For a zero-mean stationary continuous vibration signal *x(t)*, the autocorrelation function $R_{xx}(\tau)$ and the auto-power spectrum $S_{xx}(f)$ are Fourier transform pairs according to Wiener-Khinchin theorem (Couch, et al. 2001), and can be estimated by Equations (4) and (5) and as follows;

$$R_{xx}(\tau) = E\{x(t+\tau)x^*(t)\} \quad (4)$$

$$S_{xx}(f) = E\{X(f)X^*(f)\} = E\{|X(f)|^2\} \quad (5)$$

where $E\{.\}$ denotes a statistical expected value operator, $X(f)$ is the Fourier transform of $x(t)$, and superscript $*$ denotes a complex conjugate. Auto-power spectrum, $S_{xx}(f)$, describes how the mean square power of the vibration signal is distributed over frequency space.

Case Study: Using Digital Models to Detect and Recover Cavitation

When the pressure at the inlet of the pump falls below the vapor pressure of water, vapor bubbles are formed. When these vapor bubbles pass through high pressure regions at impeller outlet, they collapse and emit high energy that can damage the internal parts of the pump. Cavitation results in reducing pump head, capacity and efficiency and may damage the impeller, hence, degradation of pump life. Cavitation may be considered as the most serious problem in centrifugal pumps. Digital models, using CFD, can detect cavitation in centrifugal pumps by visualizing the pressure field and, hence, a safe range of operation can be recommended at a specific flowrate and rotational speed.

Many of researchers investigated the performance and cavitation of centrifugal pumps using CFD numerical models. Pande, et al. (2015), developed 3D simulation of turbulent fluid flow to predict velocity and pressure fields for a centrifugal

pump with ANSYS CFX. Muttalli, et al. (2014), used The standard k-ε turbulent model to study the performance parameters of centrifugal pumps and the initiation of cavitation using ANSYS CFX. Cunha and Nova (2013) presented an analytical cavitation modeling in a centrifugal pump impeller, preceded by the analysis and validation of the model by ANSYS CFX. Rajendran and Purushothaman (2012) discussed the flow pattern, pressure distribution in the blade passage, blade loading and pressure plots in centrifugal pumps using ANSYS CFX. Kim, et al. (2012) performed a comparison between transient analysis of full-type geometry and experimental results of a small industrial centrifugal pump for reliable prediction on cavitation of a centrifugal pump. Somashekar and Purushothama (2012) used ANSYS CFX to study the cavitation inception in centrifugal pump by varying water level in the cavitation well at constant speed condition and compare the numerical results with experimental data. George and Muthu (2016) studied the effects of cavitation in the performance of centrifugal pump. Shinde and Satam (2014) carried out an experimental study for analyzing cavitation of centrifugal pump and its effect on transient hydrodynamic performance during transient operation.

Results of the CFD Analysis

First, ANSYS CFX solver is run on the flow inside the pump with cavitation model turned on and low flowrate to detect cavitation. A corrective action is then taken to increase the flow through impeller eye boundary condition to reach normal operation conditions.

Eleven points are monitored to show the development of flow through the impeller blades and diffuser vanes, Figure 8. The time step is 1.565×10^{-4} *s* (2°). The total time is 0.282 s (10 revolutions). Figure 9 shows vapor volume fraction versus time. It is obvious that the vapor volume fraction increase at the points near the leading edge of the vanes at the suction side of the impeller. As the flow runs towards the high pressure zone, vapor volume fraction decreases. The creation and vanishing of vapor volume fraction continues with time. This scenario emphasizes the mechanism of cavitation where the creation and collapse of vapor bubbles occurs at small flowrates at suction combined with higher rotational speed.

Cavitation has a severe effect on centrifugal pump degradation. It is detected using digital CFD model to minimize the experimental cost. It is related directly with vapor pressure of the working fluid. The two phase flow, water and its vapor, cavitation analysis is performed at 3150 rpm with flowrate of 15 Liter/min.

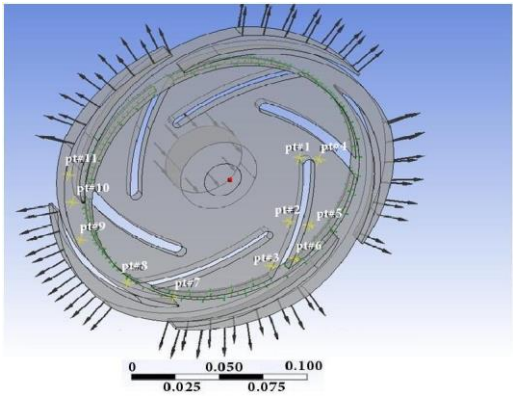

Figure 8. Schematic to Show the Eleven Monitored Points along the Impeller and Diffuser

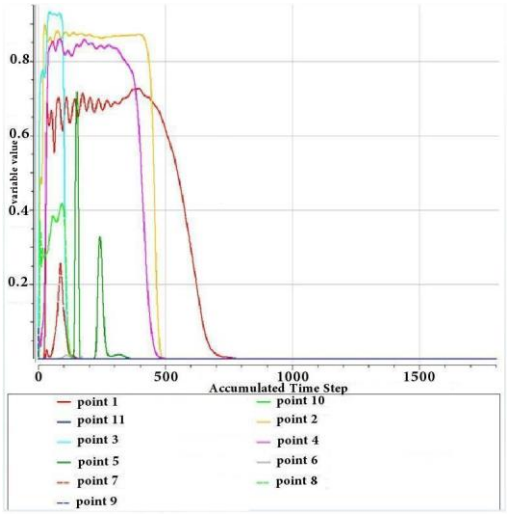

Figure 9. Vapor Volume Fraction vs. Time Step at Different Points in the Flow Zones.

Cavitation detection by CFD tools are performed in post processing by allocating the zones where pressure is lower than the vapor pressure of water, Figure 10(a). The used vapor pressure for water in the current analysis is 3170 Pa. The colored zones in Figure 10(b).are the symptoms of vapor bubbles formation. The cavitation regions appeared at the leading edge of the suction side of the impeller vanes.

As a corrective action, the flow at the inlet eye of the impeller is increased. The digital model is used to run a simulation with 55 Liter/min flowrate at inlet and 300,000 Pa at outlet of the diffuser. The pressure distribution and stream lines are shown in Figure 11.

In general the pressure increases from suction side to pressure side. While tracing the impeller flow zone, the pressure increases from the leading edge to the trailing edge as the rotational mechanical energy is converted to pressure energy.

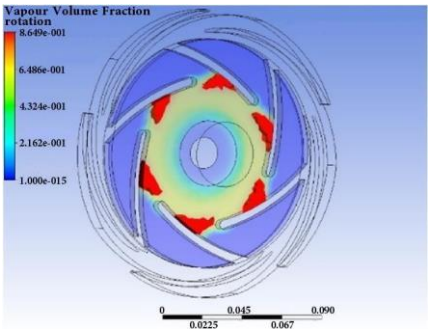

(a) Vapor Volume Fraction Contours Near Vanes Leading Edges at Suction Side.

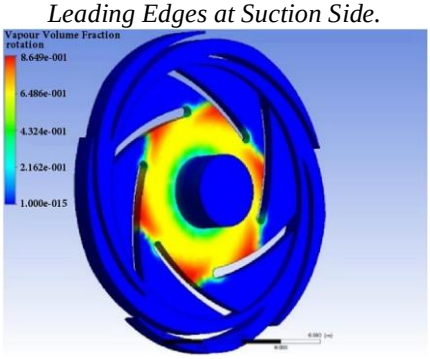

(b) Cavitation Zones Detected by Digital Model

Figure 10. Low Pressure Zones, the Pressure Drops under the Vapor Pressure of Water.

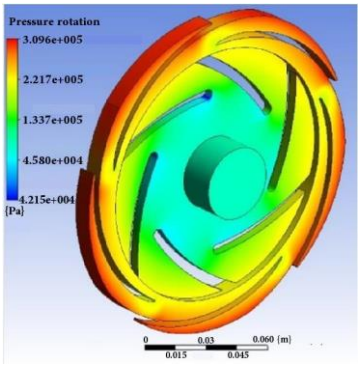

(a) Pressure Distribution in Different Flow Zones

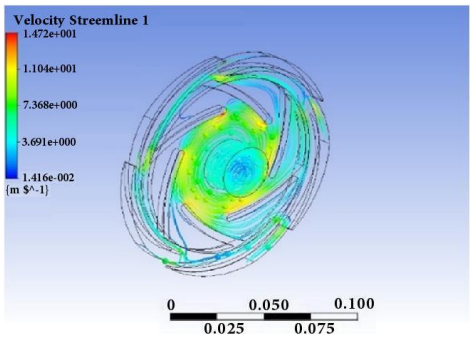

(b) Velocity Streamlines in Different Flow Zones

Figure 11. Normal Flow at 55 Liter/min. Inlet Flow and 300,000 Pa Static Pressure at Outlet.

Pressure Pulsation and Rotordynamic Response

Experimental work has previously reported that interaction between impeller blades and the diffuser results in pressure pulsation which is dominated by the Blade Pass Frequency (BPF) (Suhane 2012). This pressure pulsation is translated into force pulsation affecting the rotor through the impeller projected area. The CFD model can be used to estimate this pressure pulsation and use its resulting force as an excitation to the rotordynamic model. Response from the rotordynamic model is then compared to the accelerometer measurements collected experimentally to validate the diagnoses and to achieve better understanding of the root causes.

Figure 12 is used to illustrate how pressure pulsation is formulated due to blade-diffuser interaction. When a rotating blade approaches the diffuser tongue, it experiences a sudden drop in the pressure from level P_2 to P_1. Then, the pressure level increases monotonically until it reaches P_2 again right before next diffuser tongue. This pulse is repeated five times, number of the diffuser tongues, during one complete revolution. A good approximation of this pressure pulse within the first diffuse tongue region can be represented as a quarter of sine wave expressed mathematically as shown in Equation (6). This pressure pulse acts on the blade projected area as an exciting force to the rotating impeller. Blade projected area has to have zero value at both the beginning and the end points of the blade-diffuser interaction region. Therefore, it can be approximated in terms of half of sine wave, as shown in Equation (7). Figure 13 depicts the pressure pulsation, blade projected area, the resulting force signal acting on one blade due to blade-diffuser interaction for one complete revolution (0.02857 s). Figure 13(c) shows the normalized pressure pulsation force for one cycle. To estimate the force acting on the other impeller blades, the resulting signal force in Figure 13(c) is simply phase shifted by $2\pi/6$ for each following blade, as shown in Figure 14.

$$P_{blade1,diff.1} = P_1 + \Delta P \cos\left(\frac{5\omega t}{4}\right) \qquad 0 \le t \le 2\pi/5\omega \tag{6}$$

where ω is the impeller angular speed and $\Delta P = (P_2 - P_1)$

$$Blade\ Effective\ Area = A_0 . \sin\left(\frac{5\omega t}{2}\right) \qquad 0 \le t \le 2\pi/5\omega \tag{7}$$

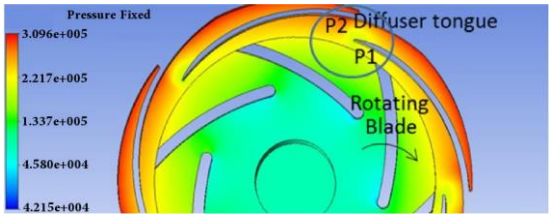

Figure 12. Pressure Distribution on Normal Operating Condition

Assuming the first blade is at zero degree angle and the six blades are equally spaced at $2\pi/6$ rad (60 degree angle), the summation of the blade forces acting on X-Y direction can be analyzed as follows:

$$F_x(t) = \sum_{i=1}^{6} F_i(t).\sin\left((i-1)\frac{2\pi}{6}\right)$$
$$F_y(t) = \sum_{i=1}^{6} F_i(t).\sin\left((i-1)\frac{2\pi}{6}\right) \quad (8)$$

where $F_i(t)$ is the force pulsation on the i^{th} blade of the impeller, as depicted in Figure 14.

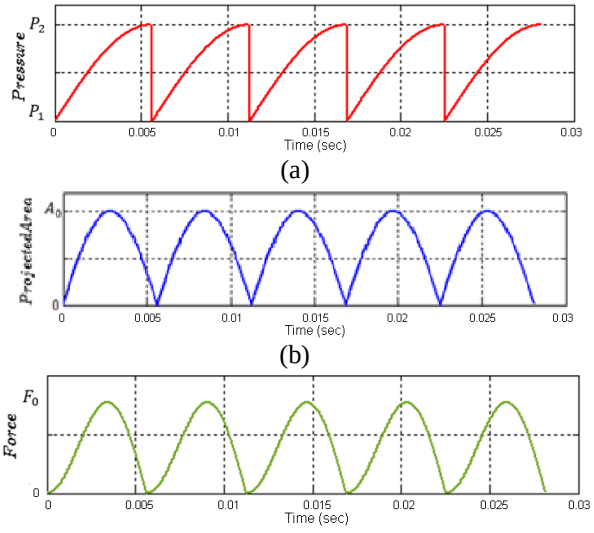

Figure 13. Pressure pulsation, projected area, and force on one blade during one complete cycle

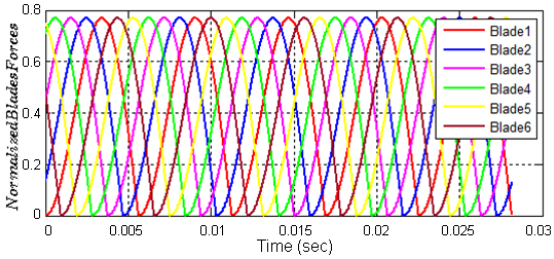

Figure 14. Normalized force pulsation on all six blades during one complete cycle

Equation (8) represents the net force on the shaft. Rotor response to this exciting force should be captured when measuring the shaft vibration on the bearings housings. This overall force is depicted in in Figure 15 (a) and (b) in time domain and frequency domain, respectively. The frequency observed at 210 Hz corresponding to the blade pass frequency (BPF) (6 x 35 Hz). It is worthwhile to note here that results of this pressure pulsation analytical model agree with experimental results obtained experimentally in (Suhane 2012).

Finally, the overall force is obtained from Equation (8) and depicted in Figure 15 is used as an excitation to the rotordynamic model. Rotor response is simulated under this condition and the (BPF) blade pass frequency (6X) is obvious in the rotor vibration, as shown in Figure 16.

Two frequencies are shown in the Figure 16. The first frequency is the synchronous (1X) vibration corresponding to the rotor unbalance. This component remains unchanged during the normal and cavitation conditions. In addition, the BPF (6X) is observed, and it is reduced in case of cavitation compared to the normal condition case.

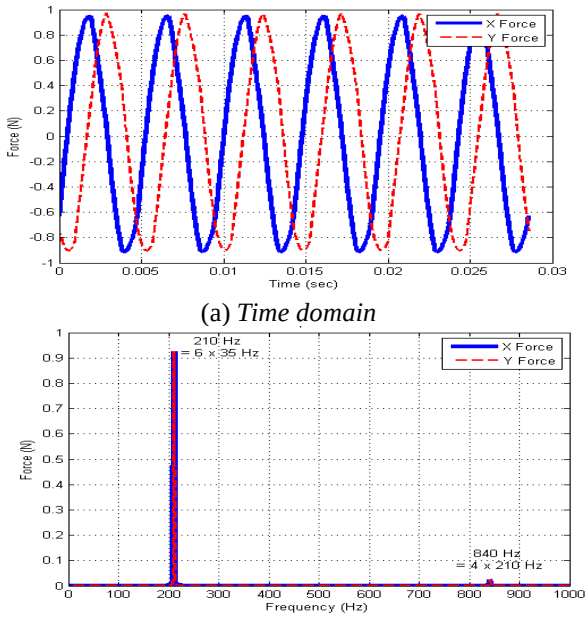

Figure 15. Overall Exciting Force in X-Y Directions

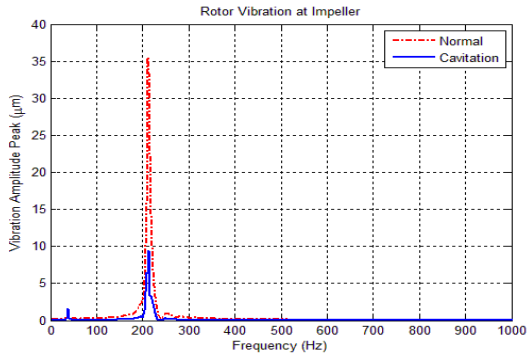

Figure 16. Rotor Response to Pressure Pulsation Force Excitation

Experimental Data Analysis

Accelerometer vibration collected from the pump and the driving motor illustrated in Figure 7 are analyzed using power spectral density described by Equation (5). Data used in this study are collected using NI compact DAQ with sampling rate of 10kHz. Vibration data are collected for one sec duration each acquisition, and for each operating condition, vibration samples are continuously collected for one minute run. Expected value operator in Equation (5) is evaluated using average over ensembles to estimate the power spectral density.

Power spectral density of the motor's vibration under normal operating condition is shown in Figure 17. Accelerometers are attached close to the motor's bearings at the driving end (DE) and non-driving end (NDE) to capture the rotordynamic response. Rotating speed recorded by tachometer is 2100rpm (35Hz). Figure 17 shows that vibration spectrum is dominated by spectral peak at 210Hz, the BPF (blade pass frequency, 6X) at both DE and NDE of the motor. This result is in a good match with that obtained from the rotordynamic model excitation force in Figure 15 and vibration response in Figure 16, and also agrees with that reported experimentally in (Suhane 2012) .

Figure 18 shows power spectral density of the motor's DE and NDE vibration collected during cavitation conditions. It is observed that spectral component at BPF shows decrease in the magnitude but it is still dominating the vibration spectrum. This result can be explained in the light of the pressure pulsation model discussed in the previous section. The exciting force affecting the rotor during cavitation must have similar frequency contents with less magnitude compared to that obtained during normal run. This decrease in the exciting force magnitude corresponds to the decrease in $\Delta P = (P_2 - P_1)$, expressed in Equation (6), as a result of the increase in P_1 due to explosion of the bubbles at this point during cavitation. Spectral peak at this BPF frequency in the DE spectrum does not show significant decrease from normal to cavitation condition. At the NDE, vibration spectrum shows decrease in the BPF magnitude by approximately -8.23dB.

Spectral signatures of the vibration signals collected experimentally are found to be in a good agreement with both the literature and the dynamic response of the digital model of rotor. The vibration excited due to pressure pulsation corresponding to the blades passing frequency is clearly observed in the measurements and simultaneously predicted in the digital models. Moreover, using the digital models help in getting more insight to the physics behind certain spectral response measured at the physical system.

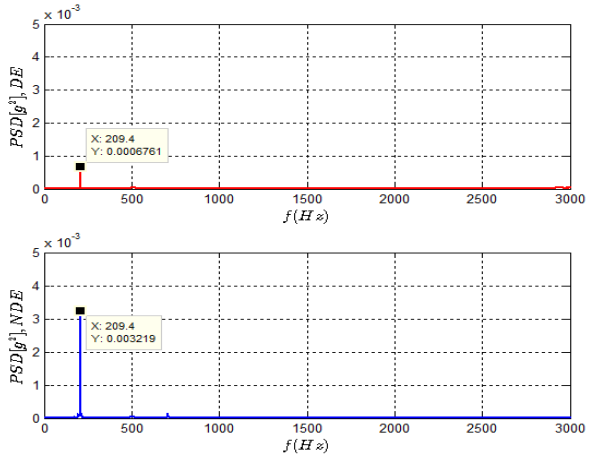

Figure 17. Power Spectrum of the Motor Vibration during Normal Run

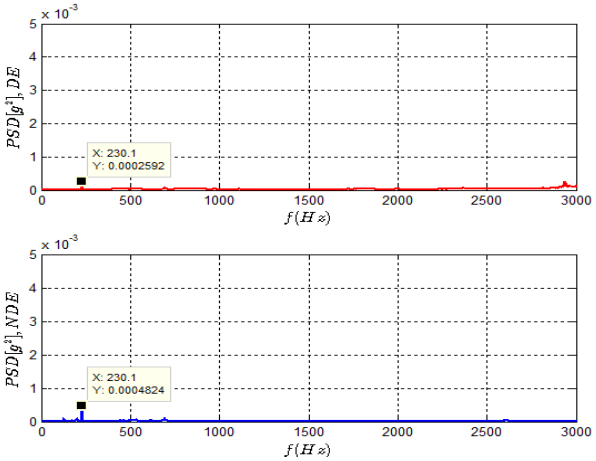

Figure 18. Power Spectrum of the Motor Vibration during Cavitation

Summary and Conclusions

In this paper, the concept of using digital model in predictive maintenance has been presented and then applied to study cavitation as a common centrifugal pump fault. First, CFD model has been built and used to study and explain the pressure

pulsation due to impeller-diffuser interaction. Resulting force is then used as an excitation to another digital model which is the rotordynamic model. Response of the rotordynamic models is finally compared to the vibration collected experimentally form the actual pump. It has been shown how digital models of the pump can be used as reliable tools for the prediction, tracking, and good understanding of root causes of common failure mechanisms in high pressure centrifugal pumps such as cavitation. Moreover, these digital models were used to virtually try different maintenance corrective actions and check which scenario works the best before applying it to the actual pump in the field. This is translated into substantial savings in both time and cost of the maintenance and ensures reliable operation of the high pressure pump.

References

Abdel-Rahman, S. M. and El-Shaikh, S. A. 2009, "Diagnosis Vibration Problems Of Pumping Stations: Case Studies," Thirteenth International Water Technology Conference, IWTC 13, Hurghada, Egypt.

Abdulkarem, W., Amuthakkannan, R., and Al-Raheem, K. F., 2014, "Centrifugal Pump Impeller Crack Detection Using Vibration Analysis," 2nd International Conference on Research in Science, Engineering and Technology (ICRSET'2014), Dubai (UAE), pp. 206-211.

Couch ,L. W., 2001, "Digital and Analog Communications Systems," (sixth ed.), New Jersey, Prentice Hall, pp. 406-409.

Cunha, M. A. and Nova, H. F., 2013, "Cavitation Modeling Of A Centrifugal Pump Impeller," 22nd International Congress of Mechanical Engineering, November 03-07.

Dewell, D.L. and Mitchell, L.D., 1984, "Detection of a Misaligned Disk Coupling Using Spectrum Analysis," Trans. ASME, Jnl of Vibration, Acoustics, Stress and Reliability in Design, Vol. 106, pp 9-18.

Farokhzad, S., Bakhtyari, N., and Ahmadi, H., 2013, "Vibration Signals Analysis and Condition Monitoring of Centrifugal Pump," *Technical Journal of Engineering and Applied Sciences*, pp. 1081-1085.

George, A. and Muthu, D. P., 2016, "CFD Analysis Of Performace Charectristics Of Centrifugal Pump Impeller To Minimising Cavitation," International Conference on Current Research in Engineering Science and Technology (ICCREST) E-ISSN :2348 - 8360 www.internationaljournalssrg.org Page 24.

Golbabaei,M., Torabi, R., Nourbakhsh, S. A., and Sedighiani, K., 2009, "Failure Detection and Optimization of a Centrifugal-pump Volute Casing," proceedings of the semiannual conference. Vol. 6(1), pp.1-6.

Hassan, M. A., Bayoumi, A. E., and Shin, Y. J., 2014, "Quadratic-Nonlinearity Index Based on Bicoherence and Its Application in Condition Monitoring of Drive-Train Components," *IEEE Transactions on Instrumentation and Measurement*, volume 63, pp. 719-728.

Hassan, M. A., Tarbutton, J., Bayoumi, A. and Shin, Y. J., 2014, "Condition Monitoring of Helicopter Trail-Rotor Drive-Shafts Using Quadratic-Nonlinearity Metric Based on Cross-Bispectral Analysis," *IEEE Transactions on Aerospace and Electronic Systems*, volume 50, pp. 2819-2829.

Kallesøe, C. S., Cocquempot, V., and Izadi-Zamanabadi, R., 2006, "Model Based Fault Detection in a Centrifugal Pump Application," IEEE Transactions on Control Systems technology, Vol. 14, No. 2.

Kim, M. J., Jin, H. B., and Chung, W. J., 2012, "A Study on Prediction of Cavitation for Centrifugal Pump," International Journal of Mechanical, Aerospace, Industrial, Mechatronic and Manufacturing Engineering Vol: 6, No:12.

Lu, J., Yuan, S., Parameswaran, S., Yuan, J., Ren, X., and Si., Q., 2017, "Investigation on the vibration and flow instabilities induced by cavitation in a centrifugal pump," *Advances in Mechanical Engineering*, volume 9, pp. 1-12.

McKee, K., Forbes, G. , Mazhar, I., Entwistle, R., and Howard, I., 2011, "A review of major centrifugal pump failure modes with application to the water supply and sewerage industries, in Asset Management Council (ed)," ICOMS Asset Management Conference, Gold Coast, QLD, Australia.

Muttalli, R. S., Agrawal, S., Warudkar, H., 2014, "CFD Simulation of Centrifugal Pump Impeller Using ANSYS-CFX," International Journal of Innovative Research in Science, (IJIRSET) ISSN: 2319-8753, Vol. 3, Issue 8.

Pande, R. M., Kandharkar, S. U., Patthe, R. B., Nandedkar, V. M., Tungikar, V. B., 2015,

"Computational Fluid Dynamics (CFD) of Centrifugal Pump to Study the Cavitation Effect," International Journal on Theoretical and Applied Research in Mechanical Engineering (IJTARME), ISSN (Print): 2319-3182, Volume -4, Issue-2.

Piotrowski, J., 1996, "Why Shaft Misalignment Continues to Befudle and Undermine Even the Best CBM and Pro-Active Maintenance Programs," Proc. Of The Predictive Maintenance Technology National Conference, Indianapolis, In 5: 18-23.

Rajendran, S. and Purushothaman, D. K., 2012, "Analysis of a centrifugal pump impeller using ANSYS-CFX," International Journal of Engineering Research & Technology (IJERT) ISSN: 2278-0181, Vol. 1 Issue 3.

Sakthivel, N.R., Sugumaran, V., and Babudevasenapati, S., 2010, "Vibration Based Fault Diagnosis of Monoblock Centrifugal Pump using Decision Tree," Expert Systems with Applications 37, pp. 4040–4049.

Shi, W., Wang, C., Wang, W., Pei, B., 2017, "Numerical Calculation on Cavitation Pressure Pulsation in Centrifugal Pump," *Advances in Mechanical Engineering*, volume 6, pp. 1-8.

Shinde, P. and Satam, A., 2014, "Cavitation Effect in Centrifugal Pump," International Journal of Researchers, Scientists and Developers, Vol. 2 No. 2 April 2014, ISSN: 2347-3649.

Somashekar, D. and Purushothama, D. H. 2012, "Numerical Simulation of Cavitation Inception on Radial Flow Pump," IOSR Journal of Mechanical and Civil Engineering (IOSRJMCE) ISSN : 2278-1684 Volume 1, Issue 5, pp. 21-26.

Suhane, A., 2012, "Experimental Study on Centrifugal Pump to Determine the Effect of Radial Clearance on Pressure Pulsations, Vibrations and Noise," International Journal of Engineering Research and Applications Vol. 2, Issue4, pp.1823-1829.

Xu, Y., Tan, L., Liu, Y., and Cao, S., 2017, "Pressure fluctuation and flow pattern of a mixed-flow pump with different blade tip clearances under cavitation condition," *Advances in Mechanical Engineering*, volume 9, pp. 1-12.